Climate Dynamics (2020) 54:3475–3487
https://doi.org/10.1007/s00382-020-05185-7

Multidecadal to decadal variability in the equatorial Indian Ocean subsurface temperature and the forcing mechanisms

Sandeep Mohapatra[1,2] · **C. Gnanaseelan**[1] · **J. S. Deepa**[1,2]

Received: 15 October 2019 / Accepted: 20 February 2020 / Published online: 28 February 2020

Abstract
The Tropical Indian Ocean (TIO) is seen to exhibit robust warming after the 1950s. Most of the previous studies on the Indian Ocean (IO) surface and subsurface temperature focussed on long-term trends and interannual variability. The multidecadal to decadal variability in the Eastern Equatorial Indian Ocean (EEIO, 80°E–110°E, 8°S–5°N, 50-110 m) subsurface temperature is studied using reanalysis products and ocean general circulation model (OGCM) simulations. Prior to 1990s, the EEIO subsurface temperature is found to be dominated mostly by the multidecadal variability. However, since the mid-1990s, significant decadal variability is observed, something that has not been reported before. The mechanisms responsible for the observed decadal and multidecadal variability in the EEIO subsurface temperature are studied in detail. Wind forcing along the equator, and the associated ocean dynamics are found to be the major factors responsible for the EEIO subsurface temperature variability in the decadal and multidecadal time scales, emphasizing the importance of local atmospheric forcing on this variability. Alongshore winds along the Sumatra coast also contribute considerably to the decadal changes in the EEIO subsurface temperature. It is also found that the observed decadal and multidecadal changes are independent of the phase reversal of Interdecadal pacific oscillation (IPO). OGCM sensitivity experiments also suggest that the decadal variability of EEIO subsurface temperature is largely unaffected by the oceanic pathways such as Indonesian Through Flow (ITF). Hence, remote forcing through these pathways is insignificant in the TIO subsurface temperature north of 10°S as compared to the TIO wind forcing. Consistent with EEIO subsurface temperature, equatorial IO (EIO) winds also exhibit decadal variability post mid-1990s. The major contributors for the decadal variability in EIO winds are found to be the decadal variability in the Mascarene high, the low level jet, and the large scale off-equatorial circulations.

Keywords Subsurface temperature · Eastern equatorial Indian Ocean · Decadal variability · Interdecadal pacific oscillation · Mascarene high

1 Introduction

Tropical Indian Ocean (TIO) is warming at a faster rate as compared to other tropical oceans since the 1950s (e.g. Du and Xie 2008; Alory and Meyers 2009). Recent studies (e.g. Dong et al. 2016; Han et al. 2014) have shown significant decadal and multidecadal variability in TIO temperature. Studies explicitly addressing the decadal/multidecadal climate variability of the Indian Ocean (IO) are few, unlike that of the Pacific (e.g. Alexander 2010; Mantua et al. 1997) and Atlantic Oceans (e.g. Liu 2012). For instance, some observational and modelling studies (e.g. Ashok et al. 2004; Schoenefeldt and Schott 2006; Tozuka et al. 2007; Han et al. 2014; Dong et al. 2016; Thompson et al. 2016) discuss the existence of multidecadal variability in the IO. In a recent study, Dong and McPhaden (2017) attributed decadal variability of TIO to anthropogenic forcing, aerosols and volcanic eruptions. It is important to note that decadal and multidecadal variability is observed in the IO subsurface temperature as well as the ocean heat content (OHC) (e.g. Trenary and Han 2008; Levitus et al. 2009; Xue et al. 2012; Han et al. 2014; Ummenhofer et al. 2017; Thompson et al. 2016). Interdecadal Pacific Oscillation (IPO) and Pacific Decadal Oscillation (PDO) are known to modulate the TIO through both oceanic and atmospheric pathways. Ummenhofer et al. (2017) and Zhou et al. (2017) argue that

✉ C. Gnanaseelan
seelan@tropmet.res.in

[1] Indian Institute of Tropical Meteorology, Pune 411008, India

[2] Savitribai Phule Pune University, Pune 411007, India

the Indonesian Through Flow (ITF) forced by PDO is the major contributor for the observed subsurface variability in the southern IO. Recently, several studies (e.g. Nieves et al. 2015; Lee et al. 2015) showed large increase in the ITF transport during the global warming hiatus period, but subsurface changes and decadal variability are only observed south of 10°S (e.g. Zhou et al. 2017). South-eastern IO is found to be affected by oceanic Rossby waves originating in the Pacific (e.g. Vaid et al. 2007; Rahul and Gnanaseelan 2016), ITF (e.g. Nieves et al. 2015; Lee et al. 2015; Rahul and Gnanaseelan 2016; Ummenhofer et al. 2017), and local surface forcing (e.g. Li et al. 2018). In contrast, decadal/multidecadal variability in the southwestern TIO (SWTIO) is found to be modulated by the surface wind forcing due to Pacific variability and the associated ocean dynamics (e.g. Han et al. 2017; Deepa et al. 2018, 2019). IPO modulates the IO sea surface temperature (SST) in decadal time scale by changing the surface heat fluxes and the thermocline through atmospheric forcing (e.g. Dong et al. 2016). Prior to 1985, both the IO basin mode and IPO show strong (positive) correlation. However, after 1985, the relationship between these two climate modes weakened (e.g. Han et al. 2014).

Like the IPO and PDO over the Pacific, climate modes over the Atlantic Ocean such as Atlantic Multi-decadal Oscillation (AMO) also influence the TIO climate through an atmospheric bridge (e.g. Li et al. 2016). However, the impact of AMO on TIO has been reported to reduce since the 1990s, mainly due to the increased external forcing and anthropogenic aerosols (e.g. Luo et al. 2018). In fact, some recent studies show that since the 1990s, the decadal variability in IO SST has affected the climate regimes in the North Atlantic (e.g. Bader and Latif 2005; Sanchez-Gomez et al. 2008; Han et al. 2014) and the Pacific (e.g. Deser and Phillips 2006; Luo et al. 2012; Han et al. 2014; Mochizuki et al. 2016) through tropical and extra-tropical atmospheric teleconnections via Walker and Hadley circulations. In this light, it is evident that in the recent decades the TIO has begun to influence the global ocean on a larger scale, thereby drawing global attention.

The vertical structure of the Eastern Equatorial Indian Ocean (EEIO) is very crucial for the interannual and decadal modulation of the Indian Ocean Dipole (IOD) (e.g. Annamalai et al. 2005). Ummenhofer et al. (2013) further reported the impact of remote wind forcing from the Pacific on the eastern IO subsurface (50–320 m) OHC variability during the IOD events. Additionally, the wind forcing associated with the IOD does not influence the decadal changes observed in the equatorial northern Indian Ocean (e.g. Thompson et al. 2016). Therefore, in the present study, detailed analysis is carried out to understand the multidecadal and decadal variability in the EEIO subsurface temperature. We also explored the relative contributions of IO forcing and remote forcing from the Pacific on the variation of the EEIO subsurface temperature in the decadal and multidecadal timescale using observations, reanalysis products, and ocean general circulation model (OGCM) simulations and sensitivity experiments. We also showed the different processes contributing to the emergence of decadal variability in the subsurface temperature over the EEIO, post mid-1990s. Section 2 describes the ocean model used for the current study and the design of the different model sensitivity experiments. The main results are discussed in Sect. 3 while Sect. 4 summarizes and discusses the major findings.

2 Model, data and methods

2.1 Model details and experiments

The OGCM used in this study is the Modular Ocean Model (MOM5), which is broadly utilised for understanding the ocean climate system (Griffies et al. 2004). The model is configured for the global domain with a horizontal resolution of 1° and 50 vertical levels with 10 m resolution in the top 250 m and the model has been forced by the Coordinated Ocean-ice Reference Experiments (CORE) forcing datasets for global ocean-ice modelling (Large and Yeager 2009) except the surface winds. The surface winds are from European Centre for Medium Range Weather Forecasts (ECMWF) Reanalysis (ERA) for the period 1958–2017, which is a merged product of ERA40 (Uppala et al. 2005) and ERA-Interim (Dee et al. 2011). As the CORE forcing is available only up to 2009, National Centers for Environmental Prediction (NCEP) reanalysis 2 products are used to force the model from 2010 to 2017. The model has been spun up from state of rest with climatological CORE Normal Year Forcing (NYF) over a period of 50 years. Further the model is integrated forward from 1958 to 2017 with interannually varying forcing fields and is referred to as CTL. The model also includes tidal mixing which is very strong in the ITF region (Koch-Larrouy et al. 2007) and so will represent the Pacific impact on the IO through oceanic pathway more realistically. The model simulations are similar to Deepa et al. (2019).

To study the impact of Pacific Ocean on IO through oceanic pathways, the surface forcing fields over the Pacific is modulated in a separate experiment (NYF-PO), which is same as the CTL except that the climatological forcing is applied over the Pacific Ocean instead of interannual forcing fields. In order to overcome the boundary effects, smoothing is done on the forcing fields over a grid region of 10° longitudes centred along the boundary lines of Indo-Pacific basins. It is important to note here that most of the grid points on which the smoothing is applied lie on the land areas and so may not have any impact on the model simulation. In addition to NYF-PO, one more experiment

(NYF-EIO), is carried out by applying NYF (of surface wind only) over the equatorial Indian Ocean (EIO; 40°E–100°E, 10°S–5°N) to quantify the role of EIO on the subsurface variability in the EEIO region. To avoid the boundary effects, smoothing is done around the boundary lines of EIO over a grid region of 10° longitudes and 5° latitudes. The experiments NYF-PO and NYF-EIO are consistent with the OGCM experiments of Ummenhofer et al. (2013).

2.2 Data sets used and methodology

Global gridded observational and reanalysis data sets are used to analyse the decadal and multi-decadal changes in the surface and subsurface of TIO. Extended Reconstructed SST version 5 (ERSSTv5; Huang et al. 2017) for the period 1900–2017 is used for analysis. The subsurface temperature data sets are taken from Ocean Reanalysis System4 (ORAS4) for the period 1958–2017. ORAS4 employs the variational ocean data assimilation system NEMOVAR using Nucleus for European Modelling of the Ocean (NEMO) version 3.0 ocean model. A detailed description of ORAS4 product and its evaluation techniques are provided by Balmaseda et al. (2013). A recent study by Karmakar et al. (2018) reported ORAS4 as one of the best reanalysis products over IO. The surface wind data considered for this work are taken from ERA-40 for the period 1958–1978 and ERA Interim for 1979–2017. The merged wind product of ERA-40 and ERA Interim data is also used for understanding the different processes in this study.

The anomalies of different variables are computed by subtracting the monthly mean climatology for the period 1958–2017 from the respective monthly fields. In the present study, ORAS4 monthly subsurface temperature data is used to calculate the thermocline depth which is defined as the depth of 23 °C isotherm (D23). Here we have preferred to use D23 instead of depth of 20 °C isotherm (D20) since the maximum temperature gradients are found along the 23 °C isotherm, which is consistent with Chen et al. (2016). The empirical orthogonal function (EOF) of D23 and upper 110 m ocean heat content (OHC) anomalies are computed for both inter-annual and decadal time scales. Decadal EOF is calculated after applying the 8-year low pass filter. An 8-year low pass Lanczos filter is implemented to remove the high frequency variations shorter than 8 years, which retains low frequency variations (greater than 8 years). The alongshore winds along Sumatra coast are calculated by taking an angle of 135° from the X-axis (e.g. Deshpande et al. 2014; Susanto et al. 2001). Similarly, a coastal upwelling index (CUI) is computed from the offshore component of Ekman transport as in Ndah et al. (2017). In addition to the above, decadal correlations between EEIO subsurface temperature and EIO wind, equatorial Pacific Ocean (EPO) wind, D23, alongshore wind, Mascarene high, low level jet, precipitation over Indian landmass etc. are also calculated for the period 1962–2013 and 1994–2013.

3 Results and discussions

The EOF analysis is carried out on the 8-year low pass filtered SST to understand the leading modes of decadal variability in the TIO and Pacific. A decadal basin mode of SST variability over the TIO (IOBM) is seen as the leading mode of decadal variability explaining 58% of the decadal variance (Fig. 1a). Similarly, in the Pacific, IPO is found to be the dominant decadal variability in SST explaining 31% of the variance (Fig. 1b). These are consistent with the previous studies (e.g. Han et al. 2014; Dong and McPhaden 2017). Figure 1c shows the corresponding principal components (PC1).

Though the recent changes in TIO SST are attributed to anthropogenic impact (e.g. Dong and McPhaden 2017), the physical processes responsible for these changes are not yet established completely. As the model simulation and reliable reanalysis products for temperature of different vertical levels are available only from 1958 onwards, we have here considered subsurface temperature of 1958–2017 for multidecadal and decadal studies. We have first examined the composite of SST anomalies during the two epochs 1958–1979 (epoch-1) and 1980–2014 (epoch-2, Fig. 2a, b). Epoch-2 is limited up to 2014 to avoid the influence of strong El Niño episode of 2015–16. A basin wide surface cooling with maximum cooling over CEIO (central equatorial Indian Ocean) is observed in epoch-1, whereas in epoch-2, a basin wide warming with maximum warming over CEIO is seen. In close association with the basin wide SST pattern, surface winds show opposite pattern (Fig. 2a, b), especially over the region south of 5°N with maximum signals over the CEIO (displaying easterly anomalies in epoch-1 and westerly anomalies in epoch-2). The anomalous wind patterns (easterlies/westerlies) are in fact favourable for strong equatorial upwelling and downwelling respectively in epoch-1 and epoch-2. These are evident in the thermocline tilt anomalies as well. Equatorial easterly wind anomalies in epoch-1 contribute to thermocline tilt anomalies with shallower thermocline in the EEIO, while equatorial westerly wind anomalies in epoch-2 lead to opposite thermocline tilt anomalies with deeper thermocline in the EEIO (Fig. 2).

It is noteworthy that anomalous patterns are seen in the subsurface temperature as well with stronger amplitudes in the depth range of 50–110 m (Fig. 2c–f) with epoch-1 displaying cooling and epoch-2 showing warming. Figure 2c, d shows the 50–110 m average temperature during the above two epochs. It is important to note the close association between the subsurface pattern seen especially in the EEIO and the SST pattern during these epochs. Further,

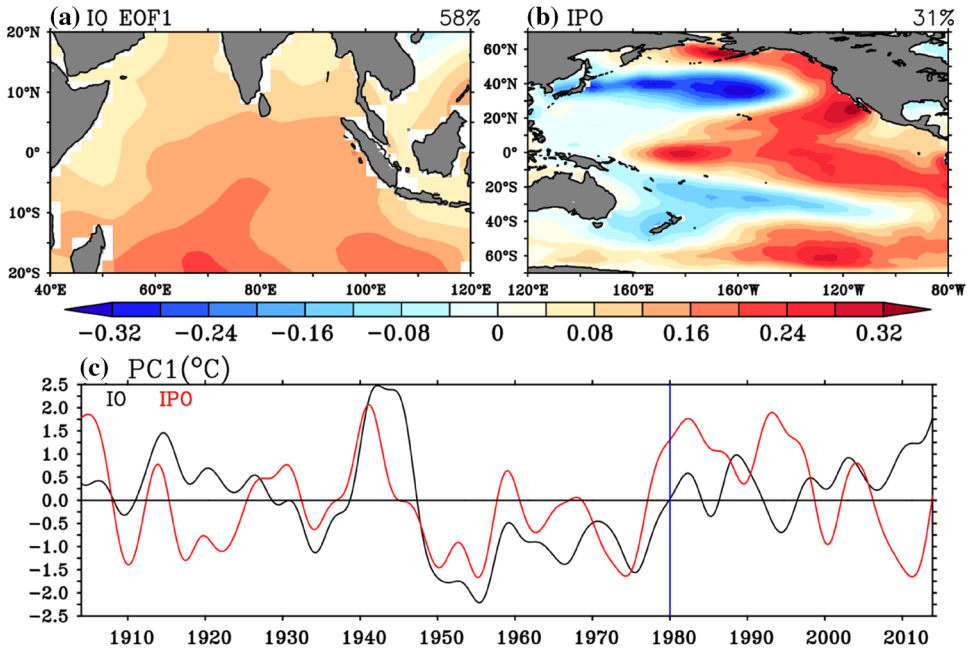

Fig. 1 The leading mode of decadal variability (EOF-1) of SST (°C) over (**a**) Indian Ocean and (**b**) Pacific Ocean from ERSST data. The values mentioned at the top right corner are the percentage of variance explained by IOBM and IPO respectively. **c** The corresponding principal component (PC1). Black line represents the PC1 of decadal IOBM and the red line shows the PC1 of IPO. Eight years low pass filter has been applied on SST anomalies after removing the long-term trend from 1900–2017. Consistently to the above, decadal EOF has also been reported by Han et al. (2014) for the period 1900–2008 by using HADISST dataset (e.g. Dong and McPhaden 2017; Han et al. 2014)

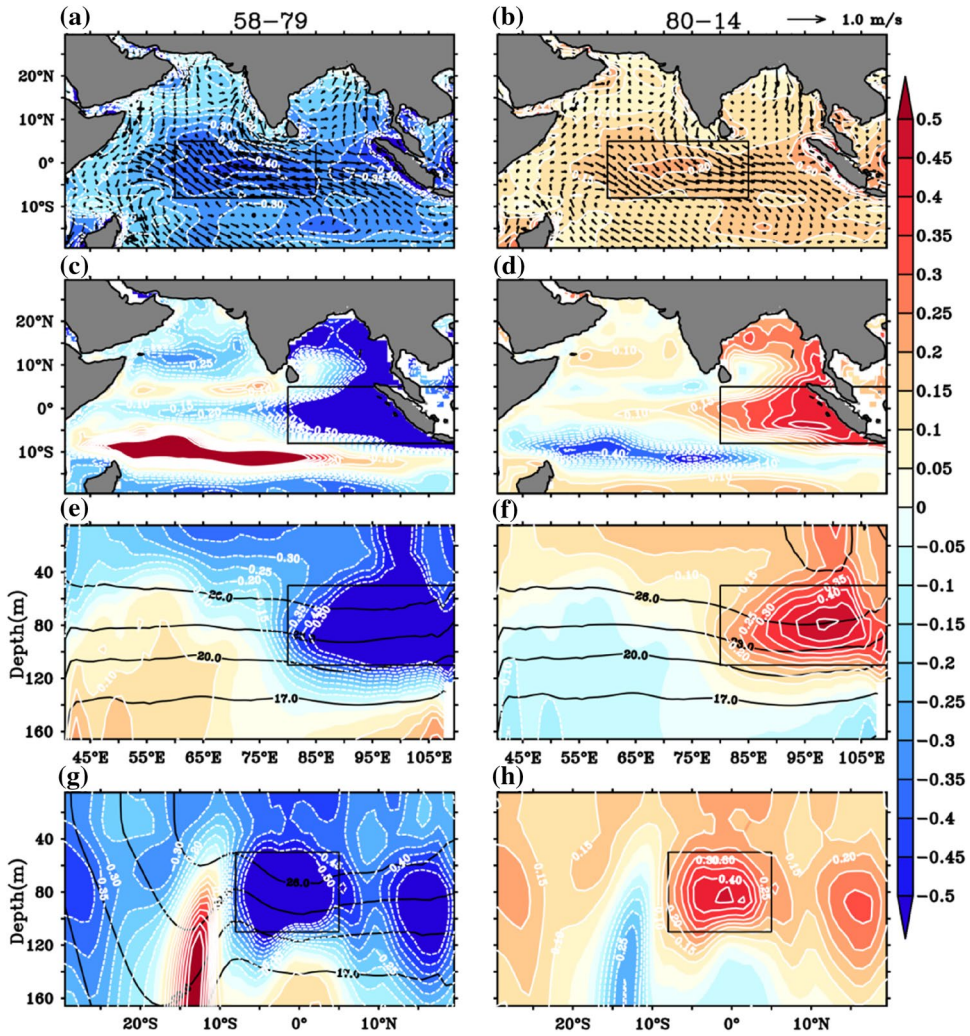

Fig. 2 Spatial and vertical structure of temperature anomaly composite (°C, shaded) in epoch-1 and epoch-2 from ORAS4. **a**, **b** SST anomaly composites (shaded) over IO in two epochs overlaid with surface wind vector composite. The highlighted box 60°E–85°E, 8°S–5°N shows prominent signals, (**c**, **d**) temperature anomaly composite averaged over 50–110 m. Here the highlighted box is 80°E–110°E, 8°S–5°N. **e**, **f** Depth-longitude plot of upper 160 m temperature anomaly composite (shaded) with mean temperature as contour (averaged over 8°S–5°N). Here the highlighted box is 80°E–110°E, 50–110 m. **g**, **h** Depth-latitude plot of upper 160 m temperature anomaly composite (shaded) with mean temperature as contour (averaged over 80 E–110 E). Here the highlighted box is 8°S–5°N, 50–110 m. The temperature anomaly composites are significant at 99% confidence level based on two-tailed Student's *t*-test (white contour). Solid (dashed) white contours represent the significance for positive (negative) temperature anomaly composite

the 3-dimensional structure of subsurface temperature over EEIO has been examined in detail. Figure 2e, f shows the depth-longitude structure of temperature anomaly composite (averaged over 8°S–5°N, where the amplitudes of subsurface signals are maximum) in the two epochs. Similarly Fig. 2g, h shows the depth latitude diagram averaged over 80°E–110°E. The subsurface cooling pattern in epoch-1 and warming pattern in epoch-2 in the eastern half of the TIO are found to be confined to the region EEIO (80°E–110°E, 8°S–5°N, 50–110 m). Hereafter EEIO refers to the above region of interest.

It is important to note that the anomalies of opposite sign are observed in the southwestern TIO (SWTIO), the Seychelles-Chagos thermocline dome region (e.g. Hermes and Reason 2008) where the thermocline is very sensitive to wind forcing and Rossby wave (e.g. Alory and Meyers 2009). Moreover, the composites shown in Fig. 2 are significant at 99% confidence level based on Student's *t*-test. OGCM simulations and sensitivity experiments and reanalysis data sets are used to further understand the processes associated with EEIO subsurface temperature evolution. It is important to mention here that the model control (CTL) simulates the anomalous subsurface features very well (Fig. 3), especially along the EEIO region, though there is an overestimation of temperature in the SWTIO and underestimation in the northern Bay of Bengal. Hence, the model CTL simulations and carefully designed sensitivity experiments are further used to understand the processes responsible for the evolution of subsurface temperature in EEIO. The ocean currents in the model are consistent with strong equatorial upwelling in epoch-1 and downwelling in epoch-2, and supporting the subsurface cooling and warming respectively (Fig. 3e, f). In close association with these equatorial upwelling and downwelling and the associated thermocline slope, strong westward and eastward surface currents (up to about 60 m) are also seen in epoch-1 and epoch-2 respectively. To further investigate the role of open ocean processes and upwelling/downwelling along EEIO in the subsurface variability, wind stress curl (shaded) and Ekman pumping (contour) for the two epochs are shown in Fig. 4. The negative (positive) wind stress curl in the south eastern EIO support strong open ocean upwelling (downwelling) during epoch-1 (epoch-2) (Fig. 4a, b). These are well supported by the Ekman pumping (contour) in the southeastern EIO region.

Several studies in the recent past have shown decadal and multidecadal time scale modulation of IO temperature by Pacific variability via ITF, especially in the region south of

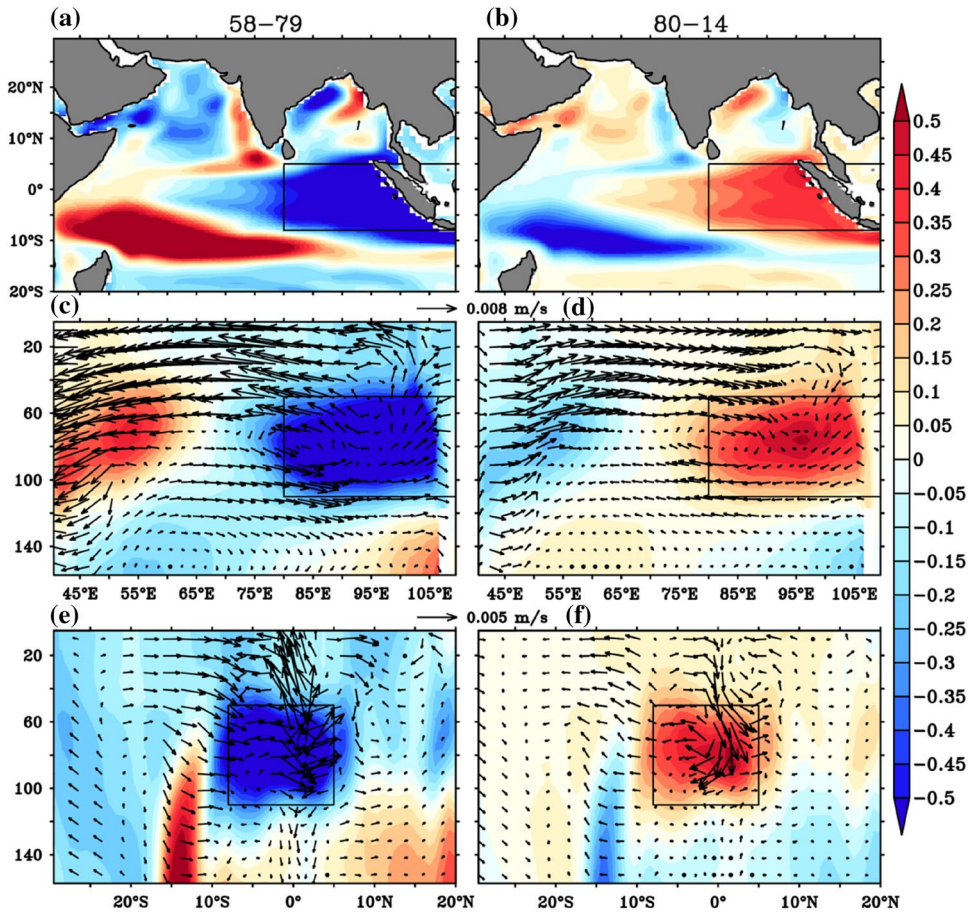

Fig. 3 Same as in previous Fig. 2 (**c**–**h**) but from MOM CTL run. **a**, **b** Spatial structure of temperature anomaly composite averaged over 50–110 m during epoch-1 and epoch-2. **c**, **d** Depth-longitude plot of upper 160 m temperature anomaly composite (shaded, °C) (averaged over 8°S–5°N) overlaid with zonal and vertical (x10e4) currents (vector, m/s). **e**, **f** Depth-latitude plot of upper 160 m temperature anomaly composite (shaded, °C) (averaged over 80°E–110°E) overlaid with meridional and vertical (x10e4) currents (vector, m/s)

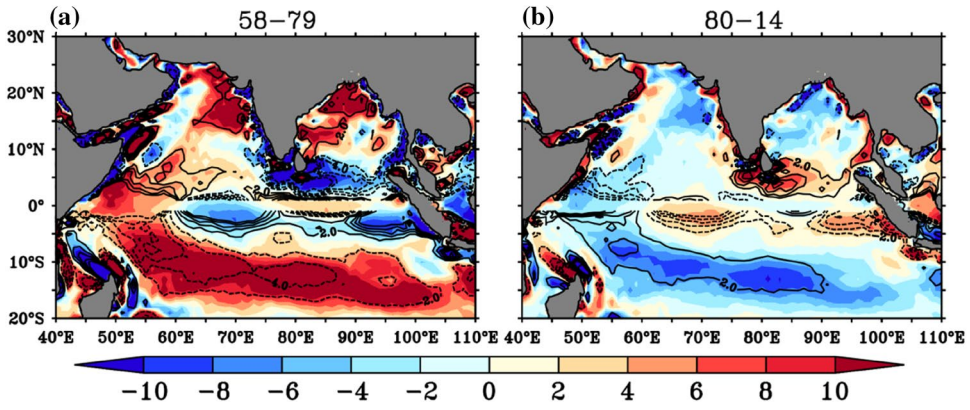

Fig. 4 **a**, **b** Composite of wind stress curl anomaly (10e-9 N/m^3, shaded) and the Ekman pumping anomaly (10e-7 m/s, contour) during the two epochs

10°S (e.g. Ummenhofer et al. 2017; Zhou et al. 2017). To examine whether there is any such role of Pacific through ITF on the EEIO temperature, we have carried out a sensitivity experiment by applying normal year forcing over the Pacific (NYF-PO). The observed subsurface temperature along EEIO in CTL and NYF-PO are found to be similar (Fig. 5a, b), thus ruling out the possibility of any significant Pacific influence on the study region through oceanic pathways. Further, it suggests that the Pacific forcing via atmospheric bridge or TIO local forcing is primarily influencing the EEIO temperature. To investigate this further, an additional experiment is carried out where the wind forcing over EIO is suppressed (NYF–EIO) in the OGCM forcing. The CTL minus NYF–EIO therefore displays the impact of EIO winds on the subsurface temperature. It is very clear from Fig. 5c, d that the EEIO subsurface variability in CTL and CTL minus NYF-EIO are similar suggesting that the EEIO subsurface temperature is mainly forced by the EIO wind forcing. It is also important to note that model subsurface temperature anomalies evolved consistently with ORAS4 during the entire study period (Fig. 6) and the epochs considered in this study are two phases of a multidecadal oscillation. The shift around 1980 may be part of a climate change trend. The correlation between ORAS4 and CTL subsurface temperature of EEIO is found to be 0.94 (Fig. 6a). To understand whether only the long term trends are the responsible factors, we examined the pattern after removing the long term trends (or detrended) from the EEIO subsurface temperature. It is found that EEIO subsurface temperature exhibits a decadal/multidecadal variability (Fig. 6b), which is different from any known variability in the EEIO. The EEIO subsurface temperature is found to retain the multidecadal and decadal variability (Fig. 6b) in NYF-PO as in CTL. Further, the decadal correlation between ORAS4

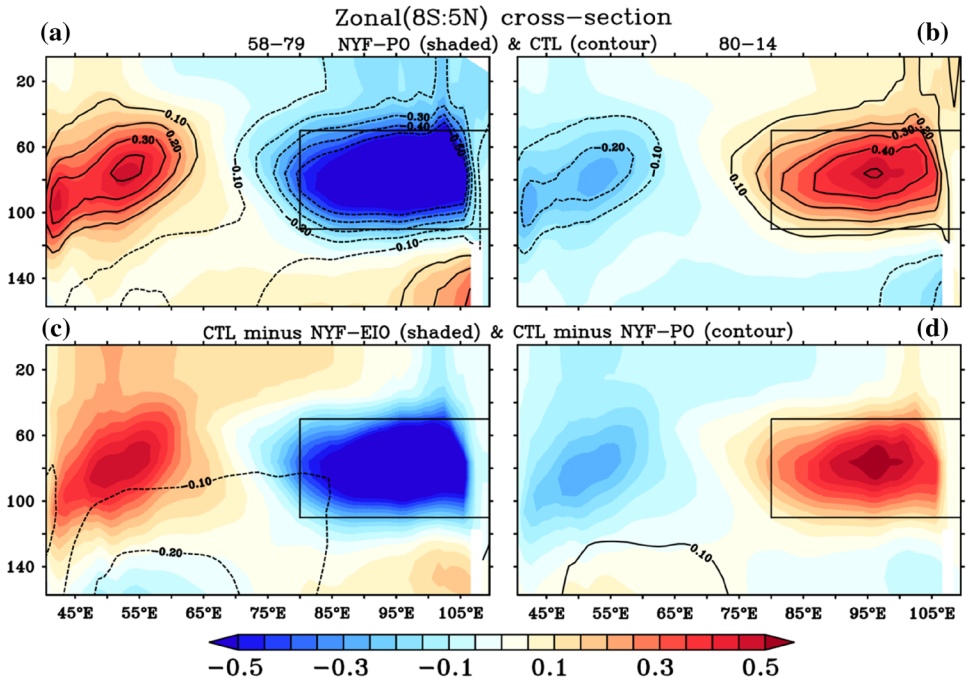

Fig. 5 Depth-longitude plot for upper 160 m temperature anomaly composite (°C) averaged over 8°S–5°N from (**a**, **b**) NYF-PO (shaded) and CTL (contour), (**c**, **d**) CTL minus NYF-EIO (shaded) and CTL minus NYF-PO (contour) during the two epochs

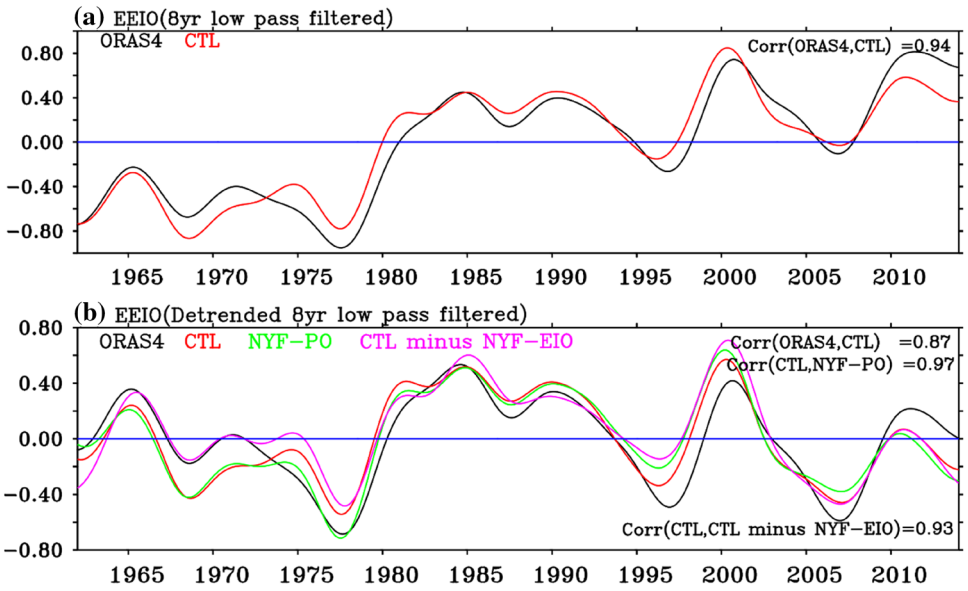

Fig. 6 Time series of 8 years low pass filtered (**a**) EEIO (80°E–110°E, 8°S–5°N) 50–110 m temperature anomaly (°C) from ORAS4 (black) and CTL (red) and (**b**) detrended temperature anomaly (°C) from ORAS4 (black), CTL (red), NYF-PO (green) and CTL minus NYF–EIO (pink)

and CTL subsurface temperature over EEIO is found to be 0.87 (Fig. 6b), which clearly suggests that the model is able to capture the EEIO subsurface temperature pattern very well. The decadal correlation between CTL and NYF-PO subsurface temperature is found to be 0.97 suggesting the negligible role of Pacific forcing through oceanic pathways (Fig. 6b). The role of EIO winds on the evolution of EEIO subsurface temperature is further evident from the decadal correlation of CTL and CTL minus NYF-EIO (r = 0.93). To further understand whether EEIO subsurface temperature is dominated by multidecadal or decadal variability, wavelet analysis is carried out for the EEIO subsurface temperature (Fig. 7). It is evident from the spectral energy peaks that the temperature in the study region exhibits decadal and multidecadal variability. It is important to highlight here that EEIO subsurface temperature is largely dominated by the multidecadal variability throughout the time period whereas post mid 1990s displayed the emergence of decadal variability. To the best of our knowledge this has not been reported before.

To further support the model experiments, statistical analysis is carried out by taking the decadal temporal

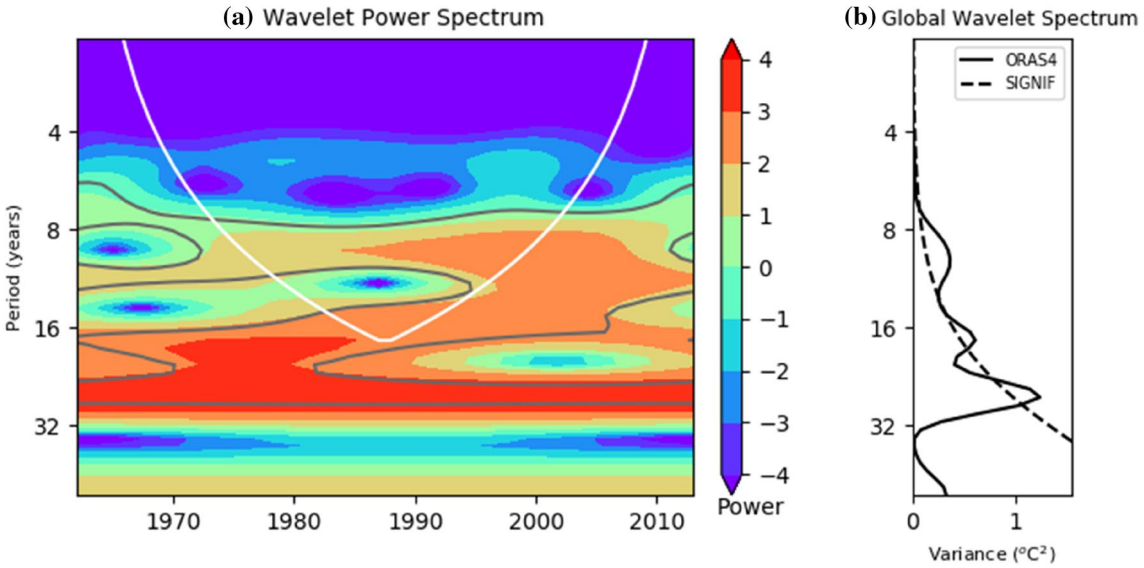

Fig. 7 Wavelet analysis of 8 years low pass filtered detrended EEIO (80°E–110°E, 8°S–5°N) 50–110 m temperature anomaly (°C) from ORAS4. **a** Wavelet power spectrum (shaded), significant at 95% confidence level (gray contour). The white curve represents the cone of influence. **b** Global wavelet spectrum (black), significant at 95% confidence level (black dotted)

correlation of EEIO subsurface temperature with the zonal wind over the entire Indo-Pacific region (Fig. 8a) on the 8-year smoothed fields. A strong positive correlation with EEIO subsurface temperature is seen over the EIO indicating a significant connection between zonal wind especially over the western and central EIO (CEIO) in decadal timescale (Fig. 8a). To further investigate the underlying dynamics causing the decadal changes in subsurface temperature and to trace whether the wind forcing is by the Pacific variability or generated internally over IO, a decadal temporal correlation between zonal wind over EIO (40°E–100°E, 5°S–5°N) and zonal wind over Indo-Pacific region is shown in Fig. 8b. The winds over EIO are found to be strongly correlated with the zonal wind over the equatorial Pacific indicating the possible connection between the winds over EIO and equatorial Pacific. To further verify the impact of remote forcing via atmospheric bridge, the IPO index (PC-1) and the time series of averaged EEIO subsurface temperature are compared (Fig. 8c). It is found that IPO leads EEIO with positive correlation between IPO and EIO before the mid 1980s and negative correlation in the post 1980s. Figure 8d shows that the IPO index is strongly correlated with zonal winds over the western EIO (WEIO) with weaker extension to CEIO. This suggests that IPO may influence EIO winds through large scale circulation changes, say Walker circulation but is mostly limited to the WEIO. In addition to that the winds over EPO are also strongly (weakly) correlated with WEIO (CEIO) winds (Fig. 9a), which is consistent with the relationship to IPO index. Our analysis suggests that the EIO winds are largely influenced by the EPO winds prior to the mid 1980s (Fig. 9b), whereas the influence of Pacific wind forcing on the TIO has been weakened in the post 1980s (Fig. 9c), which indicates that the recent changes observed over EIO is mostly driven by local internal forcing over the IO region. It is noteworthy that the Mascarene high, known as an important driver of south west monsoon exhibits similar decadal variability and is consistent with Feba et al. (2019). Our study reveals that the decadal variability in Mascarene high (MASCwind), Low Level Jet (LLJ) and off equatorial circulations (anticyclonic and cyclonic circulations respectively during the decades of equatorial easterlies and westerlies) closely associated with monsoon rainfall over India (e.g. Wang et al. 2003; Chakravorty et al. 2014) are the primary factors for the decadal modulation of EIO winds especially in the post mid 1990s (Fig. 9d). Above analysis clearly suggests that the EPO winds (mostly by IPO) contribute to the multidecadal variability in EIO winds prior to the 1990s (Fig. 9b, c), whereas the recent

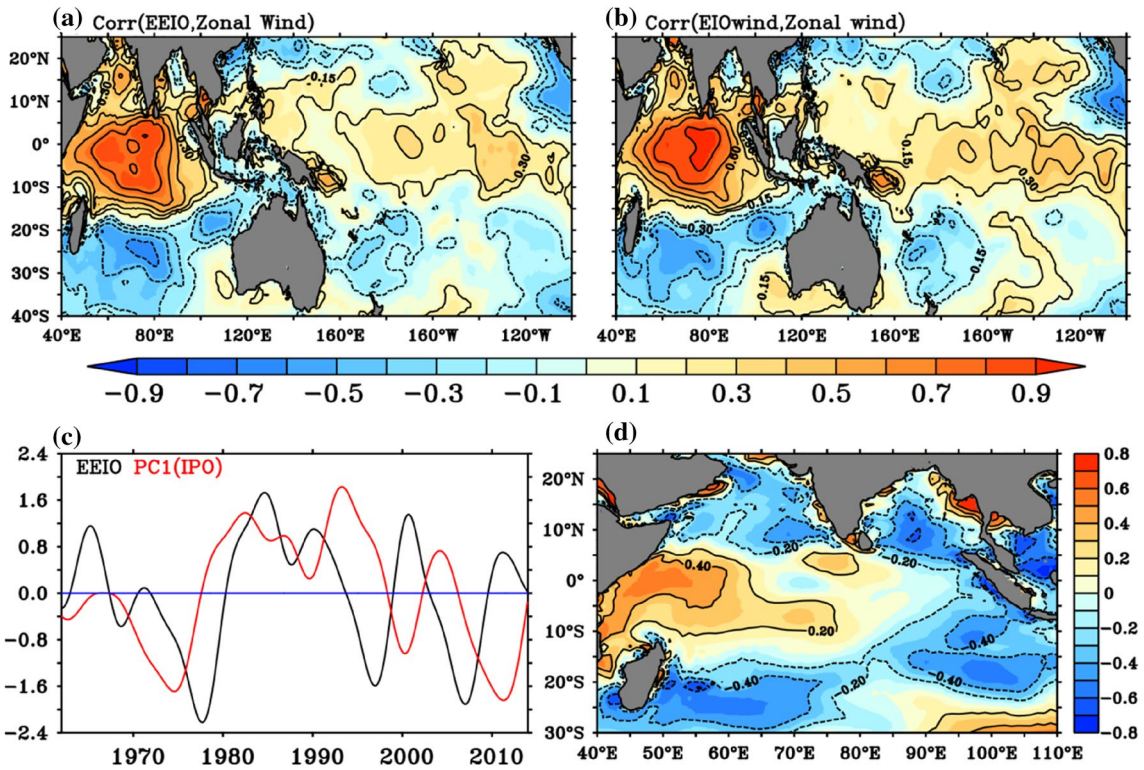

Fig. 8 Decadal temporal correlation of (**a**) EEIO subsurface temperature with zonal wind over Indo-Pacific region and (**b**) EIO zonal wind (EIOwind) with the zonal wind over Indo-Pacific region. **c** Time series of normalised decadal IPO PC1 (red line) with normalised EEIO subsurface temperature (black line), (**d**) decadal correlation of Indian Ocean zonal wind with IPO PC1 (shaded). The correlations shown in Fig a, b, d are significant at 99% confidence level based on two-tailed Student's *t*-test (contour)

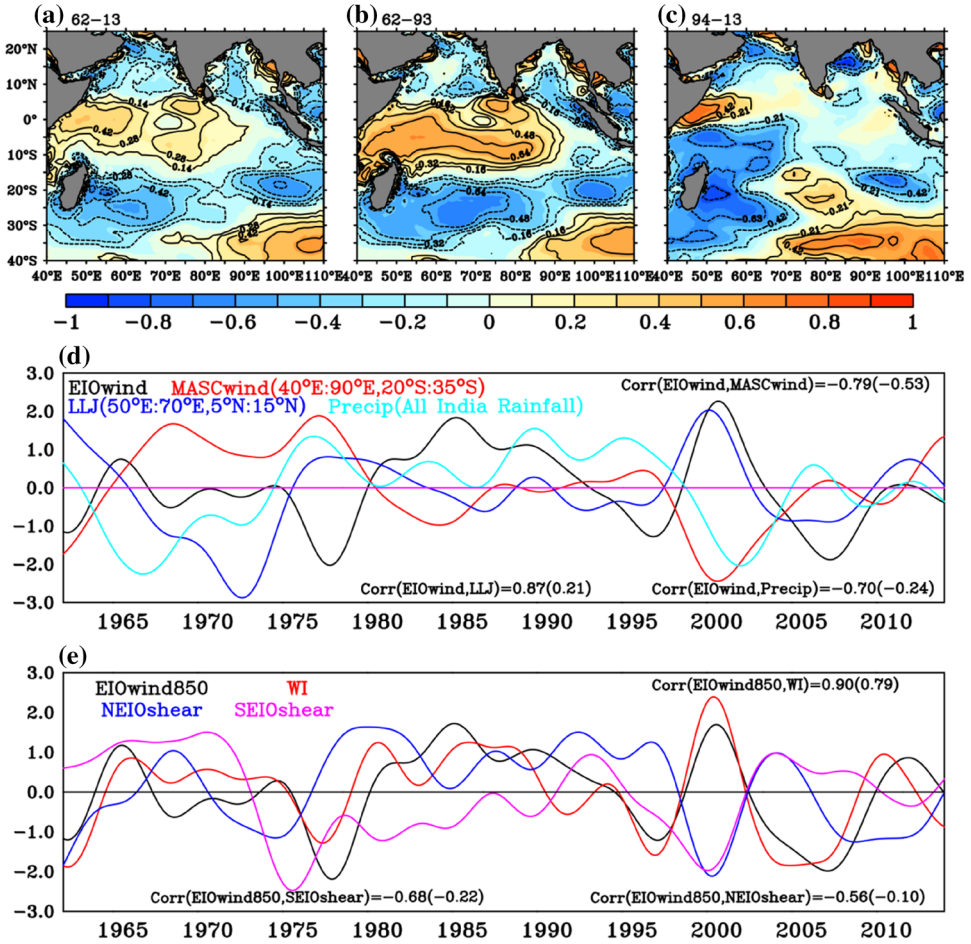

Fig. 9 Decadal correlation of zonal wind with equatorial Pacific zonalwind (averaged over 160°E–100°W, 5°S–5°N) (shaded) for the period (**a**) 1962–2013, (**b**) 1962–1993, (**c**) 1994–2013. The correlations shown in Fig a, b, c are significant at 99% confidence level based on two-tailed Student's *t*-test (contour). **d** Time series of normalized detrended 8 years low pass filtered EIO (averaged over 40°E–100°E, 5°S–5°N) wind anomaly (EIOwind, black line), 850 hPa wind anomaly over Mascarene region (MASCwind, red line), Low Level Jet (LLJ, 850 hPa wind, blue line), Precipitation anomaly (Precip, over Indian Land mass, cyan line). **e** Time series of normalized 8 years low pass filtered detrended 850 hpa EIO wind ($EIOwind_{850}$, black line), and 850 hPa wind-index (WI, red line), NEIO vertical shear (NEIOshear, blue line), SEIO vertical shear (SEIOshear, pink line). The decadal correlation (**d**, **e**) has been calculated for the period 1994–2013 (significant at 99% confidence level) and 1962–2013 (shown in brackets). NEIOshear (80°E–100°E, 10°N–20°N) and SEIOshear (80°E–110°E, 15°S–25°S) are computed based on the 200 hPa and 850 hPa zonal wind difference. Here $WI = EIOwind_{850} - (NEIOwind_{850} + SEIOwind_{850})$

emergence of decadal variability over EIO winds posterior to the mid 1990s is largely driven by local internal forcing over the IO region (contributed by the decadal variability in the MASCwind, LLJ and the associated variability in the rainfall over Indian landmass). The decadal correlations of EIO winds with MASCwind (850 hPa zonal wind averaged over 40°E:90°E, 35°S: 20°S) is −0.79, LLJ (850 hPa zonal wind averaged over 50°E:70°E, 5°N:15°N) is 0.87 and all India rainfall is −0.70 during the period 1994–2013 provide further evidence for the recent dominance of decadal variability in EIO winds and the associated mechanisms. The decadal vertical wind shear over north eastern IO (NEIO, 80°E:100°E, 10°N:20°N) and south eastern IO (SEIO, 80°E:110°E, 25°S:15°S) are correlated with EIO winds with the respective correlation coefficient of − 0.56 and −0.68 and are found to influence the decadal variability of EIO winds especially from the late 1990s (Fig. 9e). The decadal evolution of a wind index ($WI = EIOwind_{850} - (NEIOwind_{850} + SEIOwind_{850})$), defined to quantify the strength of the off-equatorial anticylconic/cyclonic circulations in both the hemispheres, has further supported our hypothesis (correlation between WI and $EIOwind_{850}$, r = 0.90). The above discussions clearly indicate that the multidecadal and decadal variability in the surface wind forcing along EIO, is the primary forcing mechanism for the long-term variability observed in EEIO subsurface temperature. In addition to this, the statistical analysis is found to be consistent with our findings. i.e. all the decadal correlations

(shown in Fig. 9) during the period 1994–2013 are found to be significant as compared to that of 1962–2013. Our findings show the significant impact of local forcing on the EIO temperature and winds in the recent years (since the mid 1990s). To further investigate the relationship between thermocline and OHC of upper 110 m in the decadal time scale, the time series of D20, D23, the upper OHC (0–110 m) and subsurface OHC (50–110 m) are shown in Fig. 10a. D23 is found to be more consistent with the upper 110 m OHC and subsurface OHC compared to D20 especially over EEIO (Fig. 10a). Chen et al. (2016) also found maximum vertical temperature gradient in the EEIO at D23. So D23 is chosen as the thermocline depth for the remainder of the paper. From decadal correlation analysis it is more evident that D23 along EEIO is closely associated with EEIO subsurface temperature (r = 0.99, and is shown in Fig. 10a). Consistent with D23, over EEIO, the upper 110 m OHC (r = 0.95 with D23) and 50–110 m OHC (r = 0.99, with D23) are closely related to D23 and exhibit similar decadal variability (Fig. 10a). The above analysis clearly suggests that the upper 110 m OHC is highly influenced by subsurface temperature rather than temperature in the depth range 0–50 m. Previous studies reported the interannual variability in the CEIO winds (e.g. Gadgil et al. 2004) and the associated variability in ocean circulation (e.g. Thompson et al. 2006; Gnanaseelan et al. 2012). Here we report the existence of decadal and multidecadal variability of EIO winds (Figs. 9d, 10b). Wind induced thermocline along the equator (D23, averaged over 2°S–2°N) shows a pattern similar to that of EEIO subsurface temperature, which is more evident from the Fig. 11. Alongshore winds and coastal upwelling index (CUI) along the Sumatra coasts are also examined to understand their contribution on EEIO subsurface temperature variability and to see whether they display any decadal characteristics. It is important to note that along with EIO winds both alongshore winds and CUI consistently contribute to the EEIO subsurface temperature variability with maximum impact observed since the mid 1990s. We also quantified the role of decadal wind stress curl (W_{curl}) over SEIO and its close association with the EEIO variability during the last two decades. The decadal correlation of EEIO subsurface temperature with EIO wind (r = 0.90), alongshore wind (r = −0.39), CUI (r = −0.36), D23 (r = 0.96) and W_{curl} (r = −0.36) are significant at 99% confidence level based on two-tailed student's *t*-test. The above analysis clearly indicates that the wind forcing is mainly driving the decadal and multidecadal variability in the subsurface temperature as compared to the remote forcing from the Pacific Ocean through ITF via oceanic pathways. Consistent with Fig. 10b, D23 anomaly along the equator both from CTL and ORAS4 are consistent with the equatorial wind, suggesting a strong upwelling/downwelling over EEIO (Fig. 11a, b). The Hovmoller diagram

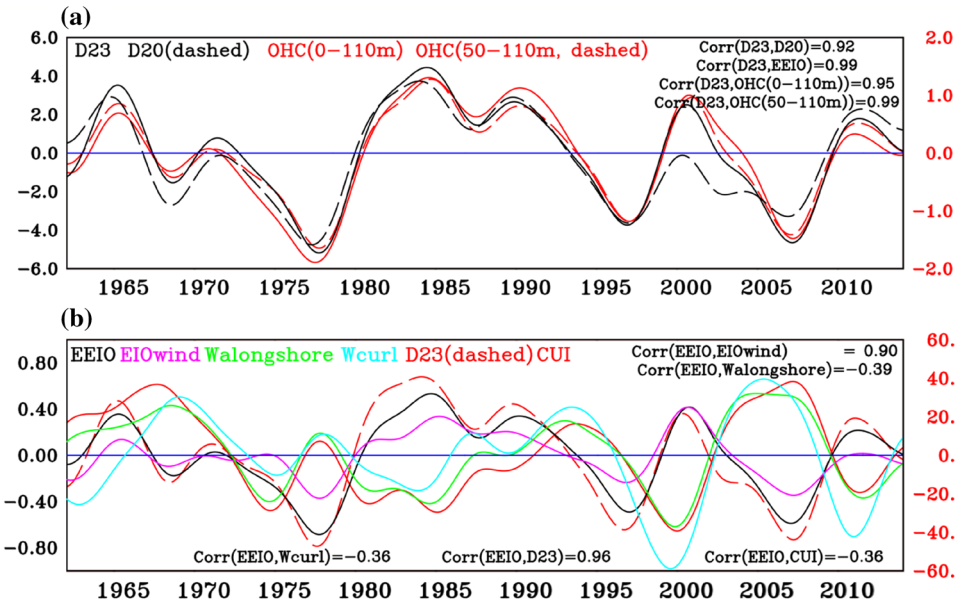

Fig. 10 **a** Time series of 8 years low pass filtered detrended D23 anomaly (m, solid black line), D20 anomaly (m, dashed black line) and upper 110 m oceanic heat content anomaly (10e8 J/m^2, solid red line) and 50–110 m oceanic heat content (10e8 J/m^2, dashed red line) averaged over 80°E–110°E, 8°S–5°N. **b** Time series of detrended 8 years low pass filtered EEIO subsurface temperature anomaly (°C, black), EIO (averaged over 40°E–100°E, 5°S–5°N) wind anomaly (m/s, EIOwind, pink line), alongshore wind anomaly (m/s, Walongshore, green line), coastal upwelling index (m^3 s^{-1} per 100 m coastline, CUI, red line), D23 anomaly (10e-1 m, 80°E–110°E, 2°S–2°N, dashed red line) and wind stress curl anomaly (10e-8 N/m^3, Wcurl, cyan line) averaged over 80°E–110°E, 15°S–25°S. The correlations between EEIO temperature and EIO wind, Walongshore, CUI, D23 and Wcurl are significant at 99% confidence level based on two-tailed Student's *t*-test

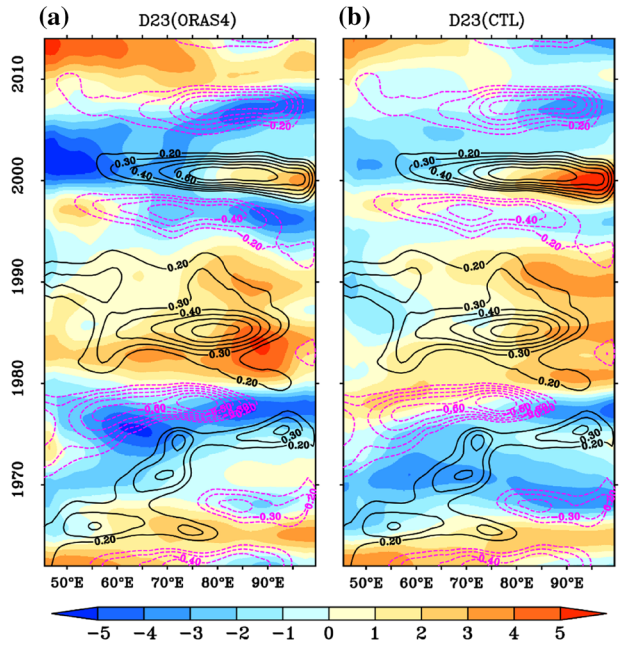

Fig. 11 Hovmoller diagram of detrended 8 years low pass filtered D23 anomaly (m, D23, shaded) averaged over 2°S–2°N from (**a**) ORAS4 and (**b**) CTL overlaid with ERA zonal wind anomaly (m/s, contour)

further suggests that the anomalous equatorial westerlies (easterlies) induce downwelling (upwelling) thus leading to thermocline tilt with deeper (shallower) thermocline anomalies over EEIO.

4 Summary and discussion

The Tropical Indian Ocean exhibits significant decadal and multidecadal temperature variability with larger amplitude over EEIO subsurface. The present study is mostly focused on the EEIO subsurface temperature variability and its internal dynamics using reanalysis products and OGCM sensitivity experiments. During the epoch-1 (1958–1979) EEIO exhibits a strong cooling whereas in the epoch-2 (1980–2014) the region is characterized by a significant warming. The above two epochs are found to be the two phases of a multidecadal oscillation and the shift around 1980 may be part of a climate change trend. The surface easterlies and westerlies in the epochs are found to cause cooling and warming in the EEIO during epoch-1 and epoch-2 respectively. Further, the atmospheric forcing along the equator is the driving force for the multidecadal and decadal changes in the subsurface temperature. The winds over the EIO play a major role in the multidecadal and decadal variability which is quite evident from the model sensitivity experiments as well. The ocean model sensitivity experiments reveal that EEIO is largely unaffected by the Pacific forcing through ITF, whereas EEIO is affected by EIO winds. In addition to EIO winds, the alongshore wind and coastal upwelling along the Sumatra coast further contribute to the decadal and multidecadal variability in EEIO. The subsurface temperature, thermocline, upper OHC (0–110 m) and subsurface OHC (50–110 m) are found to exhibit consistent decadal and multidecadal variability over EEIO.

It is evident from the analysis that the multidecadal variability is present throughout the study period, whereas the decadal variability evolves only after the mid 1990s which is being reported for the first time in this study. It is important to note that the conclusions drawn are based on the available limited period reanalysis and model simulations, and reliable long term data sets are prerequisite for understanding the multidecadal variability. The multidecadal and decadal signal observed over EEIO is evident in the wavelet power spectrum as well. Prior to the 1990s EPO winds influence the EIO winds through atmospheric pathways whereas in the recent decades the relationship between these winds over the two basins has drastically changed. Moreover, the recent decadal changes observed in EEIO temperature and EIO winds especially after the mid 1990s are mainly driven by local forcing such as low level jet (LLJ), Mascarene high and large scale off equatorial circulations (anticyclonic and cyclonic circulations respectively during the phases of equatorial easterlies and westerlies). Apart from the above, decadal precipitation over Indian land mass is also found to be closely related to that of EIO winds in the mid 1990s strongly suggesting the possible common cause. It is found that the vertical wind shear over NEIO and SEIO are further supporting the decadal nature of EIO winds from the late 1990s through modulating the off equatorial anticyclonic and cyclonic circulations. The above factors are found to be the primary forcing mechanisms for the emergence of decadal variability in the EEIO subsurface temperature in the recent decades.

Acknowledgments We thank Director, ESSO-IITM and Ministry of Earth Sciences (MoES), Government of India for the support. Sandeep Mohapatra thanks IITM for research fellowship. Comments from the anonymous reviewers have helped us to improve the manuscript. We acknowledge Deepti Gnanaseelan for language edits. ERSSTv5 data is from https://www.esrl.noaa.gov/psd/data/gridded/data.noaa.ersst.v5.html. ORAS4 temperature data is downloaded from Asia–Pacific Data Research Centre (APDRC) (http://apdrc.soest.hawaii.edu/data/data.php). ERA40 and Interim wind data at surface levels are taken from http://apps.ecmwf.int/datasets/. Figures are prepared using PyFerret and Python.

References

Alexander MA (2010) Extratropical air-sea interaction, sea surface temperature variability, and the Pacific decadal oscillation. In: Sun D, Bryan F (eds) Climate dynamics: Why does climate vary? AGU Monograph #189, Washington, pp 123–148

Alory G, Meyers G (2009) Warming of the upper equatorial Indian Ocean and changes in the heat budget (1960–99). J Clim 22(1):93–113. https://doi.org/10.1175/2008JCLI2330.1

Annamalai H, Potemra J, Murthugudde R, McCreary JP (2005) Effect of preconditioning on the extreme climate events in the tropical Indian Ocean. J Clim 18:3450–3469. https://doi.org/10.1175/JCLI3494.1

Ashok K, Chan WL, Motoi T, Yamagata T (2004) Decadal variability of the Indian Ocean dipole. Geophys Res Lett 31:L24207. https://doi.org/10.1029/2004GL021345

Bader J, Latif M (2005) North Atlantic Oscillation response to anomalous Indian Ocean SST in a coupled GCM. J Clim 18:5382–5390. https://doi.org/10.1175/JCLI3577.1

Balmaseda MA, Mogensen K, Weaver AT (2013) Evaluation of the ECMWF ocean reanalysis system ORAS4. Q J R Meteorol Soc 139:1132–1161. https://doi.org/10.1002/qj.2063

Chakravorty S, Gnanaseelan C, Chowdary JS, Luo J-J (2014) Relative role of El Niño and IOD forcing on the southern tropical Indian Ocean Rossby waves. J Geophys Res 119:5105–5122. https://doi.org/10.1002/2013JC009713

Chen G, Han W, Li Y, Wang D (2016) Interannual variability of equatorial eastern Indian Ocean upwelling: local versus remote forcing. J Phys Ocean 46:789–807. https://doi.org/10.1175/JPO-D-15-0117.1

Dee DP et al (2011) The ERA-Interim reanalysis: configuration and performance of the data assimilation system. Q J R Meteorol Soc 137:553–597. https://doi.org/10.1002/qj.828

Deepa JS, Gnanaseelan C, Kakatkar R, Parekh A, Chowdary JS (2018) The interannual sea level variability in the Indian Ocean as simulated by an ocean general circulation model. Int J Climatol 38:1132–1144. https://doi.org/10.1002/joc.5228

Deepa JS, Gnanaseelan C, Mohapatra S, Chowdary JS, Karmakar A, Kakatkar R, Parekh A (2019) The tropical Indian Ocean decadal sea level response to the Pacific decadal oscillation forcing. Clim Dyn 52:5045–5058. https://doi.org/10.1007/s00382-018-4431-9

Deser C, Phillips AS (2006) Simulation of the 1976/1977 climate transition over the North Pacific: sensitivity to tropical forcing. J Clim 19:6170–6180. https://doi.org/10.1175/JCLI3963.1

Deshpande A, Chowdary JS, Gnanaseelan C (2014) Role of thermocline–SST coupling in the evolution of IOD events and their regional impacts. Clim Dyn 43:163–174. https://doi.org/10.1007/s00382-013-1879-5

Dong L, McPhaden MJ (2017) Why has the relationship between Indian and Pacific Ocean decadal variability changed in recent decades? J Clim 30:1971–1983. https://doi.org/10.1175/JCLI-D-16-0313.1

Dong L, Zhou T, Dai A, Song F, Wu B, Chen X (2016) The footprint of the inter-decadal Pacific oscillation in Indian Ocean sea surface temperatures. Sci Rep 6:21251. https://doi.org/10.1038/srep21251

Du Y, Xie S-P (2008) Role of atmospheric adjustments in the tropical Indian Ocean warming during the 20th century in climate models. Geophys Res Lett 35:L08712. https://doi.org/10.1029/2008GL033631

Feba F, Ashok K, Ravichandran M (2019) Role of changed Indo-Pacific atmospheric circulation in the recent disconnect between the Indian summer monsoon and ENSO. Clim Dyn 52:1461–1470. https://doi.org/10.1007/s00382-018-4207-2

Gadgil S, Vinayachandran PN, Francis PA, Gadgil S (2004) Extremes of the Indian summer monsoon rainfall, ENSO and equatorial Indian Ocean oscillation. Geophys Res Lett 31:L12213. https://doi.org/10.1029/2004GL019733

Gnanaseelan C, Deshpande A, McPhaden MJ (2012) Impact of Indian Ocean Dipole and El Niño/Southern oscillation forcing on the Wyrtki jets. J Geophys Res 117:C08005. https://doi.org/10.1029/2012JC007918

Griffies SM, Harrison MJ, Pacanowski RC, Rosati A (2004) A technical guide to MOM4. GFDL Ocean group technical report No. 5, Princeton NJ NOAA/Geophysical fluid dynamics laboratory pp 342

Han W, Vialard J, McPhaden MJ, Lee T, Masumoto Y, Feng M, Ruijter WPM (2014) Indian Ocean decadal variability: a review. Bull Am Meteorol Soc 95:1679–1703. https://doi.org/10.1175/BAMS-D-13-00028.1

Han W, Meehl GA, Hu A, Zheng J, Kenigson J, Vialard J, Rajagopalan B, Yanto (2017) Decadal variability of the Indian and Pacific Walker cells since the 1960s: Do they covary on decadal time scales? J Clim 30:8447–8468. https://doi.org/10.1175/jcli-d-16-0783.1

Hermes JC, Reason CJC (2008) Annual cycle of the South Indian Ocean (Seychelles–Chagos) thermocline ridge in a regional ocean model. J Geophys Res 113:C04035. https://doi.org/10.1029/2007JC004363

Huang B, Thorne Peter W et al (2017) Extended reconstructed sea surface temperature version 5 (ERSSTv5), upgrades, validations, and intercomparisons. J Clim 31:8179–8205. https://doi.org/10.1175/JCLI-D-16-0836.1

Karmakar A, Parekh A, Chowdary JS, Gnanaseelan C (2018) Inter comparison of Tropical Indian Ocean features in different ocean reanalysis products. Clim Dyn 51:119–141. https://doi.org/10.1007/s00382-017-3910-8

Koch-Larrouy A, Madec G, Bouruet-Aubertot P, Gerkema T, Bessières L, Molcard R (2007) On the transformation of Pacific water into Indonesian through flow water by internal tidal mixing. Geophys Res Lett 34:L04604. https://doi.org/10.1029/2006GL028405

Large WG, Yeager S (2009) The global climatology of an interannually varying air—sea flux data set. Clim Dyn 33:341–364. https://doi.org/10.1007/s00382-008-0441-3

Lee SK, Park W, Baringer MO, Gordon AL, Huber B, Liu Y (2015) Pacific origin of the abrupt increase in Indian Ocean heat content during the warming hiatus. Nat Geosci 8:445–449. https://doi.org/10.1038/NGEO2438

Levitus S, Antonov JI, Boyer TP, Locarnini RA, Garcia HE, Mishonv AV (2009) Global ocean heat content 1955–2008 in light of recently revealed instrumentation problems. Geophys Res Lett 36:L07608. https://doi.org/10.1029/2008GL037155

Li X, Xie S-P, Gille ST, Yoo C (2016) Atlantic-induced pantropical climate change over the past three decades. Nat Clim Change 6:275–279. https://doi.org/10.1038/nclimate2840

Li Y, Han W, Hu A, Meehl G, Wang F (2018) Multidecadal changes of the upper Indian Ocean heat content during 1965–2016. J Clim 31:7863–7884. https://doi.org/10.1175/JCLI-D-18-0116.1

Liu Z (2012) Dynamics of Interdecadal climate variability: an historical perspective. J Clim 25:1963–1995. https://doi.org/10.1175/2011JCLI3980.1

Luo J-J, Sasaki W, Masumoto Y (2012) Indian Ocean warming modulates Pacific climate change. Proc Natl Acad Sci USA 109(46):18701–18706. https://doi.org/10.1073/pnas.1210239109

Luo F, Li S, Furevik T (2018) Weaker connection between the Atlantic multidecadal Oscillation and Indian summer rainfall since the mid-1990s. Atmos Oceanic Sci Lett. https://doi.org/10.1080/16742834.2018.1394779

Mantua NJ, Hare SR, Zhang Y, Wallace JM, Francis RC (1997) A Pacific interdecadal climate oscillation with impacts on salmon production. Bull Am Meteorol Soc 78:1069–1079. https://doi.org/10.1175/1520-0477(1997)078%3c1069:APICOW%3e2.0.co;2

Mochizuki T, Kimoto M, Watanabe M, Chikamoto Y, Ishii M (2016) Inter-basin effects of the Indian Ocean on Pacific decadal climate change. Geophys Res Lett 43:7168–7175. https://doi.org/10.1002/2016GL069940

Ndah AB, Dagar L, Becek K (2017) Multi-temporal patterns of upwelling–downwelling dynamics in the South China Sea based on a 47-year time-series of the NOAA-ERD upwelling

index. Reg Stud Mar Sci 16:225–239. https://doi.org/10.1016/j.rsma.2017.08.017

Nieves V, Willis JK, Patzert WC (2015) Recent hiatus caused by decadal shift in Indo-Pacific heating. Science 349:532–535. https://doi.org/10.1126/science.aaa4521

Rahul S, Gnanaseelan C (2016) Can large scale surface circulation changes modulate the sea surface warming pattern in the Tropical Indian Ocean? Clim Dyn 46:3617–3632. https://doi.org/10.1007/s00382-015-2790-z

Sanchez-Gomez E, Cassou C, Hodson DLR, Keenlyside N, Okumura Y, Zhou T (2008) North Atlantic weather regimes response to Indian-western Pacific Ocean warming: a multi-model study. Geophys Res Lett 35:L15706. https://doi.org/10.1029/2008GL034345

Schoenefeldt R, Schott FA (2006) Decadal variability of the Indian Ocean cross-equatorial exchange in SODA. Geophys Res Lett 33:L08602. https://doi.org/10.1029/2006GL025891

Susanto RD, Gordon AL, Zheng Q (2001) Upwelling along the coast of Java and Sumatra and its relation to ENSO. Geophys Res Lett 28(8):1599–1602. https://doi.org/10.1029/2000GL011844

Thompson B, Gnanaseelan C, Salvekar PS (2006) Variability in the Indian Ocean circulation and salinity and its impact on SST anomalies during dipole events. J Mar Res 64:853–880

Thompson PR, Piecuch CG, Merrifield MA, McCreary JP, Firing E (2016) Forcing of recent decadal variability in the Equatorial and North Indian Ocean. J Geophys Res Oceans 121:6762–6778. https://doi.org/10.1002/2016JC012132

Tozuka T, Luo JJ, Masson S, Yamagata T (2007) Decadal modulations of the Indian Ocean Dipole in the SINTEX-F1 coupled GCM. J Clim 20:2881–2894. https://doi.org/10.1175/JCLI4168.1

Trenary LL, Han W (2008) Causes of decadal subsurface cooling in the tropical Indian Ocean during 1961–2000. Geophys Res Lett 35:L17602. https://doi.org/10.1029/2008GL034687

Ummenhofer CC, Schwarzkopf FU, Meyers G, Behrens E, Biastoch A, Böning CW (2013) Pacific Ocean contribution to the asymmetry in eastern Indian Ocean variability. J Clim 26:1152–1171. https://doi.org/10.1175/JCLI-D-11-00673.1

Ummenhofer CC, Biastoch A, Böning CW (2017) Multi-decadal Indian Ocean variability linked to the pacific and implications for preconditioning Indian Ocean Dipole events. J Clim 30:1739–1751. https://doi.org/10.1175/JCLI-D-16-0200.1

Uppala S et al (2005) The ERA-40 re-analysis. Q J R Meteorol Soc 131:2961–3012. https://doi.org/10.1256/qj.04.176

Vaid BH, Gnanaseelan C, Polito PS, Salvekar PS (2007) Influence of pacific on Southern Indian Ocean Rossby waves. Pure Appl Geophys 164:1765–1785. https://doi.org/10.1007/s00024-007-0230-7

Wang B, Wu R, Li T (2003) Atmosphere—warm ocean interaction and its impact on Asian-Australian monsoon variation. J Clim 16:1195–1211. https://doi.org/10.1175/1520-0442(2003)16%3c1195:AOIAII%3e2.0.CO;2

Xue et al (2012) A comparative analysis of upper ocean heat content variability from an ensemble of operational ocean reanalyses. J Clim 25:6905–6929. https://doi.org/10.1175/JCLI-D-11-00542.1

Zhou XB, Alves O, Marsland SJ, Bi Daohua, Hirst AC (2017) Multi-decadal variations of the south Indian ocean subsurface temperature influenced by pacific decadal oscillation. Tellus A 69:1–12. https://doi.org/10.1080/16000870.2017.1308055